parasitologia

MDPI

Article

Progression of *Trypanosoma cruzi* Dm28c Strain Infection in a BALB/c Mouse Experimental Model

María Azul de Hernández [1], Silvina Raquel Villar [2,3,*] and Pamela Cribb [1,4,*]

[1] Instituto de Biología Molecular y Celular de Rosario, Consejo Nacional de Investigaciones Científicas y Técnicas, Universidad Nacional de Rosario (IBR-CONICET-UNR), Rosario 2000, Argentina; dehernandez@ibr-conicet.gov.ar
[2] Facultad de Ciencias Médicas, Universidad Nacional de Rosario, Rosario 2000, Argentina
[3] Instituto de Inmunología Clínica y Experimental de Rosario, Consejo Nacional de Investigaciones Científicas y Técnicas, Universidad Nacional de Rosario (IDICER-CONICET-UNR), Rosario 2000, Argentina
[4] Facultad de Ciencias Bioquímicas y Farmacéuticas, Universidad Nacional de Rosario, Rosario 2000, Argentina
* Correspondence: villar@idicer-conicet.gob.ar (S.R.V.); cribb@ibr-conicet.gov.ar (P.C.); Tel.: +54-93416225796 (P.C.)

Abstract

Chagas disease, caused by *Trypanosoma cruzi*, presents a variety of clinical outcomes ranging from mild symptoms to Chagas cardiomyopathy, the most severe and life-threatening manifestation of the disease. The degree of virulence is influenced by both parasite and host factors. In this study, we characterized a murine infection model using the *T. cruzi* Dm28c strain in BALB/c mice to assess disease progression. Infected mice showed a peak of parasitemia at 14 dpi, followed by a progressive decrease. Spleen weight increased up to sixfold compared to uninfected controls at 14 and 21 dpi, correlating with parasitemia levels. Histological analysis revealed focal inflammatory infiltrates in the heart starting at 7 dpi, with maximal intensity at 14 and 21 dpi. The expression of inflammatory cytokines (IFN-γ, IL-1β, TNF-α) and anti-inflammatory cytokines (IL-10, TGF-β) in the spleen showed a dynamic profile, with an early increase during the acute phase. Dm28c infection of BALB/c mice can be considered as a non-lethal Chagas disease experimental model, with detectable parasitemia during the acute phase and a controlled inflammatory response.

Keywords: *Trypanosoma*; inflammatory response; parasitemia; non-lethal; spleen

Academic Editor: Vyacheslav Yurchenko

Received: 11 July 2025
Revised: 8 August 2025
Accepted: 29 August 2025
Published: 9 September 2025

Citation: de Hernández, M.A.; Villar, S.R.; Cribb, P. Progression of *Trypanosoma cruzi* Dm28c Strain Infection in a BALB/c Mouse Experimental Model. *Parasitologia* **2025**, *5*, 47. https://doi.org/10.3390/parasitologia5030047

1. Introduction

Chagas disease, also known as American trypanosomiasis, is caused by the flagellated protozoan *Trypanosoma cruzi*. Although it was first described more than a century ago, this illness still remains a major public health problem affecting more than 7 million people worldwide, with severe morbidity and leading to more than 10,000 deaths every year [1]. Chagas is endemic in 21 countries in Latin America, but in recent decades, it has acquired increasing global relevance due to migration patterns [2]. Transmission occurs primarily through direct contact with the feces of infected blood-sucking triatomine vector bugs or through the ingestion of contaminated food. Alternative routes independent of the insect vector include congenital, transfusional, and transplant-associated routes, which are of major concern in non-endemic regions. The clinical course of the disease is typically divided into an acute and chronic phase. The acute phase, often asymptomatic or presenting nonspecific symptoms such as fever and lymphadenopathy, is followed by lifelong chronic infection. Most individuals remain inan indeterminate asymptomatic form, but without

early diagnosis and treatment, approximately 30% progress to clinically evident chronic Chagas disease, primarily characterized by cardiomyopathy, although gastrointestinal forms can also occur [3]. Trypanocide treatment with the currently available drugs—Benznidazole and Nifurtimox—aims to eliminate the parasite from the body to prevent the establishment or progression of visceral damage, mainly cardiac and/or digestive. Remarkably, it helps interrupt vertical transmission when administered to women of childbearing age and if treatment is initiated early in the acute phase, Chagas disease can be cured. In contrast, during the chronic phase, treatment may help slow disease progression and reduce the risk of transmission, but we are generally unable to achieve a complete cure [4].

The clinical manifestations—both in the acute and chronic phases—and the evolution of the disease are highly variable and difficult to predict, reflecting the complex interplay between parasite, host, and environmental factors [5]. There is still ongoing debate about the specific roles of parasite genotypes and host immunological factors in the progression and prognosis of Chagas disease. Furthermore, the significant variability in infection outcomes among individuals remains largely unexplained [6,7].

A key feature of *T. cruzi* is its remarkable genetic diversity and its associated phenotypic characteristics. The parasite is currently classified into seven discrete typing units (DTUs), from TcI to TcVI and TcBat [6]. These DTUs differ in geographic distribution, reservoir associations, susceptibility to drugs, tissue tropism, and virulence. Infections with different DTUs have been associated with distinct clinical manifestations and disease outcomes [6–8]. For instance, TcI is widespread and prevalent in northern South America, Central America, and sylvatic cycles, often linked to cardiac forms of the disease. TcII, TcV, and TcVI are more common in the Southern Cone and have been associated with severe chronic cardiomyopathy and digestive syndromes. TcIII and TcIV are mostly sylvatic and less commonly implicated in human disease. TcBat, initially identified in bats, appears to be restricted to sylvatic cycles and has not been clearly associated with human infection [7,9]. This genetic diversity of *T. cruzi* is suspected to have an impact on susceptibility to drugs, although additional factors linked to the life history trait of each strain might also impact the response to therapeutic agents [10].

Similarly to other human infectious diseases, animal models play a crucial role in helping researchers to understand Chagas disease and develop new prevention and treatment approaches. Experimental models using different *T. cruzi* strains have provided valuable insights into pathogenesis. However, due to the significant genetic and phenotypic diversity of *T. cruzi* and the variability in clinical manifestation and outcomes, generalizations must be cautiously made [11].

In this study, we characterized a murine infection model using the *T. cruzi* Dm28 strain in BALB/c mice. The Dm28 strain has a sylvatic origin and was first isolated from the opossum Didelphis marsupialis. The Dm28c clone used in this study was originally selected for its ability to infect vectors and vertebrates, invade cultured cells, and differentiate in vitro, and it has been extensively characterized [12]. The Dm28 strain is classified within DTU TcI and has the capacity to establish chronic infection in mice with low-to-moderate virulence. The BALB/c mouse strain selected as the host is widely used in *T. cruzi* infection studies due to its susceptibility, which results in higher parasite loads compared to more resistant strains such as C57BL/6. It also mounts a well-characterized Th2/Th1-type immune response, which enables effective parasite control [13]. This dynamic response offers advantageous context to study cytokine regulation, immune balance, and disease progression. Moreover, BALB/c mice present a reproducible infection pattern with many *T. cruzi* strains, including a clear acute and chronic phase.

Because of the low-to-moderate virulence, the Dm28c-infection model allows for the study of disease progression through the acute to chronic phase in contrast to more virulent and highly mortal strains.

2. Materials and Methods

Mice and parasites

BALB/c male mice (6–8 weeks old) were obtained and maintained at the animal facilities of the Centro de Investigación y Producción de Reactivos Biológicos (CIPReB-FCM-UNR, Argentina). A total of 26 BALB/c mice were randomly allocated into 6 groups, as stated below. The number of animals was determined based on ethical considerations and in accordance with the 3Rs principle (Replacement, Reduction, and Refinement), ensuring the responsible use of experimental animals. Only male BALB/c mice were used to minimize variability associated with sex-related hormonal fluctuations, which can modulate immune responses and influence the course of *T. cruzi* infection. Mice were housed in ventilated racks equipped with HEPA filters under controlled humidity (40–70%) and temperature (21–23 °C). Animals were kept in plastic cages (approximately 25 × 35 cm) with grid lids and sterile wood shavings as bedding. A 12 h light/dark cycle was maintained. Sterile food and water were provided ad libitum. To minimize potential confounders, cage positions were rotated weekly to avoid location-based bias. All animal handling procedures, including cage changes and treatments, were performed in laminar flow workstations. Sample collection was conducted under anesthesia using ketamine (100 mg/kg) and xylazine (10 mg/kg), followed by euthanasia via CO_2 inhalation. Protocols for animal studies were approved by the Institutional Animal Care & Use Committee (Res. No. 2477/2016).

Trypanosoma cruzi trypomastigotes of the Dm28c strain (DTU TcI) were obtained from an in vitro infection. Briefly, Vero cells (ATCC CCL-81) were cultured in Dulbecco's Modified Eagle Medium (DMEM) (ThermoFisher, Waltham, MA, USA), and high glucose was achieved with L-glutamine and pyruvate, supplemented with 10% fetal calf serum (FCS) (Internegocios S.A., Cordoba, Argentina). Cell-derived trypomastigotes were obtained by infection with metacyclic trypomastigotes in Vero cell monolayers at an MOI of 10 parasites per cell [14]. Trypomastigotes were collected from the supernatant of the infected cell culture after 4–5 days post infection, harvested by centrifugation at 7000× *g* for 10 min at room temperature, resuspended in DMEM, and counted using a Neubauer chamber. Parasite suspensions were adjusted to the desired concentration in sterile phosphate-buffered saline (PBS) prior to the inoculation of mice.

Experimental infection

Twenty mice were infected intraperitoneally with 50,000 cell-derived trypomastigotes resuspended in 100 µL of sterile PBS and housed randomly in groups of 3 or 4 animals per cage. Four experimental groups [7, 10, 14, and 21 days post-infection (dpi)] were defined to evaluate the progression of *T. cruzi* infection in the acute phase (n = 4 for 7 and 10 dpi; n = 3 for 14 and 21 dpi) and an additional group (n= 6, divided in 2 cages) was monitored until 56 dpi to evaluate survival. An uninfected control group (n= 6, divided into 2 cages) was maintained under the same housing conditions. The general health status of all experimental groups was monitored daily up to 56 days post-infection (dpi), and no animal needed to be excluded from the analysis due to signs of suffering (animal suffering was established as an exclusion criterion a priori). Parasitemia was assessed by direct microscopic examination of peripheral blood samples according to Brener's method as described [15,16]. Blood, heart, and spleen samples were collected from all animals in each group at the indicated dpi. Organs were cut in pieces and slices were either preserved in

paraffin for histological analysis or in RNAhold® solution (TransGen Biotech Co., Beijing, China) for molecular studies. Spleens were also weighed at the time of collection.

Heart histology

Cardiac tissues obtained from euthanized animals at 7, 10, 14, 21, and 56 dpi were processed using standard histological techniques. Samples previously fixed in 4% buffered formalin and embedded in paraffin were sectioned at 5 µm thickness. Hematoxylin and eosin staining was performed at the Morphology Service of the Facultad de Ciencias Bioquímicas y Farmacéuticas, Universidad Nacional de Rosario (FBIOyF, UNR). Additionally, cardiac fibrosis was assessed using Picrosirius Red/Fast Green staining.

For each animal, 3–4 cardiac tissue sections were analyzed. Inflammatory infiltrates were evaluated based on their size and type, and a score was assigned to estimate the severity of myocarditis. The score was determined as follows: the absence of foci was scored as no inflammation, mild foci indicated slight infiltration with damage of one or two myocardial fibers, moderate foci were infiltrates compromising three to five myocardial fibers, and severe foci were dense infiltrates with destruction of more than five myocardial fibers. Additionally, the presence of amastigote nests was evaluated. Six random fields per section were analyzed at 20× magnification.

RNA Extraction and Spleen Cytokine Expression analysis

Total RNA was extracted from mouse spleens stored in RNAhold® using TriReagent® (MRC, Cincinnati, OH, USA) following the manufacturer's instructions. RNA quality and quantity were assessed by agarose gel electrophoresis and spectrophotometry (Abs260 nm/280 nm), respectively. When the total RNA sample failed quality checks, they were excluded from this analysis (excluded samples: 1 from 10 dpi, 1 from 56-dpi, and 2 from the control group).

RNA samples were treated with RQ1 RNase-free DNase (Promega Corporation, Madison, WI, USA) to remove contaminating genomic DNA before reverse transcription.

One microgram of RNA was reverse transcribed into cDNA using oligo (dT) primers and M-MLV Reverse Transcriptase (Promega Corporation, Madison, WI, USA) according to the manufacturer's protocol. Real-time PCR was performed using HOT FIREPol® EvaGreen® qPCR Supermix (Solis BioDyne, Tartu, Estonia) in a Bio-Rad CFX Maestro System (Bio-Rad Laboratories, Hercules, CA, USA). Gene-specific primers for the target cytokines (Table 1) were used for amplification. For the determination, cDNAs were diluted 1:20 using ultrapure water.

Table 1. Primers used for the analysis of cytokine mRNA expression by RT-qPCR.

Target	Forward (5′-3′)	Reverse (5′-3′)	Annealing Temperature
TNF-a	TGTGGCTTCGACCTCTACCTC	GCCGAGAAAGGCTGCTTG	60 °C
IFN-g	GGTGACATGAAAATCCTGCAG	CCTCAAACTTGGCAATACTCATGA	60 °C
IL-1b	TTGACGGACCCCAAAAGATG	AGAAGGTGCTCATGTCCTCA	55 °C
TGF-b	GCTGATCCCGTTGATTTCCA	GTGGCTGAACCAAGGAGACG	60 °C
IL-10	GGTTGCCAAGCCTTATCGGA	ACCTGCTCCACTGCCTTGCT	62 °C
RPLP0	CTCTCGCTTTCTGGAGGGTG	ACGCGCTTGTACCCATTGAT	60 °C

Messenger RNA (mRNA) levels for interferon γ (IFN-γ), interleukin 1-β (IL-1β), tumoral necrosis factor α (TNF-α), interleukin 10 (IL-10), and transforming growth factor β (TGF-β) at different dpi values were estimated using the ΔΔCt method relative to the RPLP0 gene expression (60S acidic ribosomal protein P0). For each gene, reaction specificity was confirmed by performing a melting curve analysis between 55 °C and 95 °C with continuous fluorescence measurements.

Statistical analysis

All analyses were performed using GraphPad Prism 8.0 software (GraphPad Software, Boston, MA, USA). Expression data were analyzed by the ΔΔCt method, normalized to the housekeeping gene RPLP0, and expressed relative to the uninfected control group. Results are presented as mean ± standard error of the mean (SEM) and were analyzed using unpaired Student's *t*-test. Parasitemia (trypomastigotes/50 microscopic fields) and spleen weight variations were expressed as mean ± standard deviation (SD) and analyzed by a one-way analysis of variance (ANOVA) followed by Tukey's multiple comparisons test [17]. Statistical significance was considered at $p < 0.05$. Levels of significance were indicated as follows: $p < 0.05$ (*), $p < 0.01$ (**), $p < 0.001$ (***), and $p < 0.0001$ (****).

3. Results

3.1. Parasitemia in Dm28c Infected Mice Showed a Peak at 14 Days Post-Infection and Became Undetectable by Day 56

BALB/c mice were infected intraperitoneally with 50,000 cell culture infection-derived trypomastigotes of the *T. cruzi* Dm28c strain. Infection was monitored at different days post-infection (dpi) and survival was evaluated daily up to 56 dpi.

All the animals survived throughout the entire period, showing good general health condition, with no signs of piloerection, hunched posture, ocular alterations, impaired mobility, or diarrhea. Notwithstanding the apparent "healthy" external conditions, parasitemia was detectable between 7 and 21 dpi, reaching a peak of 72 ± 28 trypomastigotes per 50 microscopic fields (mean ± SD) between 10 and 14 dpi. Thereafter, parasitemia progressively decreased, becoming undetectable by 56 dpi (Figure 1).

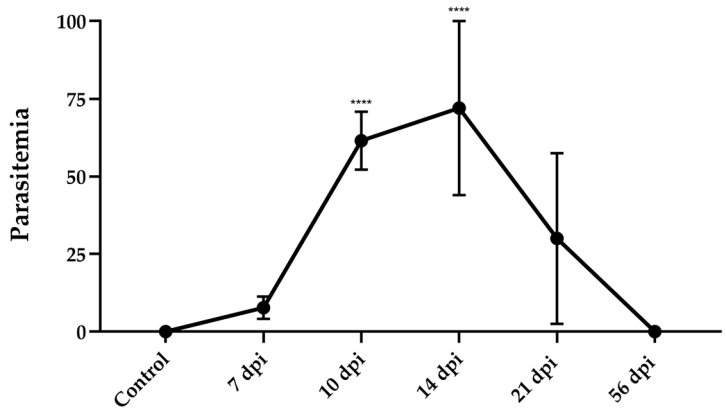

Figure 1. Blood parasitemia profile in BALB/c mice infected with 50,000 *T. cruzi* Dm28c trypomastigotes. Parasitemia curve obtained after inoculating male BALB/c mice (6–8 weeks old) with 50,000 *T. cruzi* Dm28c trypomastigotes per animal detected at different days post-infection (dpi). Data are presented as mean ± SD (n = 3–6 per group). Statistical significance was assessed by one-way ANOVA followed by Tukey's post hoc test. **** $p < 0.0001$.

3.2. Amastigote Nests and Myocarditis Signs Were Visible During Acute Infection

Heart condition was also evaluated during the study period. Histological analysis of hematoxylin-and-eosin-stained heart tissues revealed that infection with the Dm28c strain induced acute cardiomyopathy characterized by diffuse inflammatory infiltrates (Figure 2A). These infiltrates became visible from 7 dpi, when mononuclear cells progressively accumulated in the interstitial spaces. Intense inflammation was observed at 14 and 21 dpi, followed by a gradual decline (Table 2). By 56 dpi, the infiltration was mild and comparable to that observed at the uninfected control. Notably, the infiltrates appeared uniformly distributed across the cardiac tissue, with no apparent focal accumulation. Amastigote nests were also detected in the cardiac tissue and followed a similar temporal pattern with the peak of inflammation (Figure 2B). Additionally, Picrosirius Red/Fast Green

staining revealed no evidence of fibrosis at any of the analyzed time points, indicating that infection with Dm28c did not progress to fibrotic remodeling during the study period (Appendix A Figure A1).

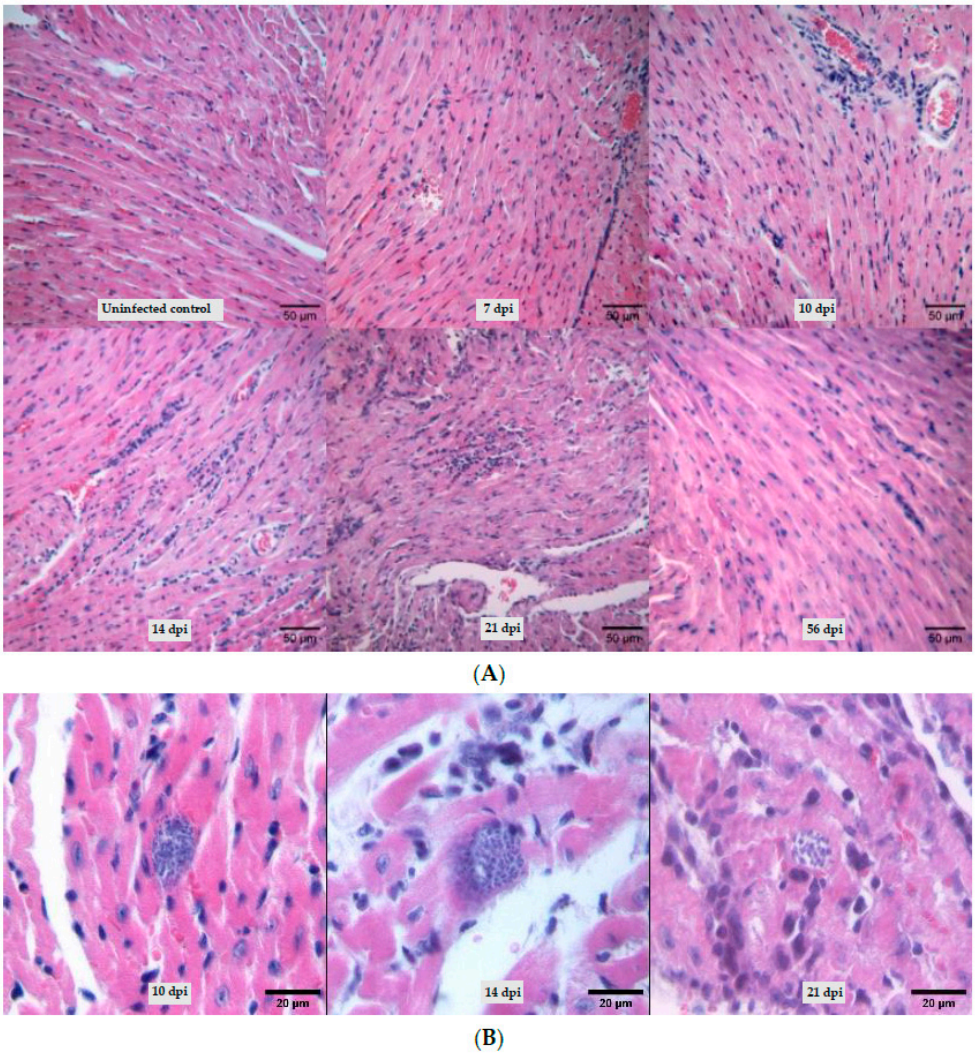

Figure 2. Histological analysis of cardiac tissue from *T. cruzi* Dm28c-infected mice. Both panels show histopathological sections of cardiac tissue stained with hematoxylin and eosin, obtained from BALB/c mice infected with 50,000 trypomastigotes per animal of the *T. cruzi* Dm28c strain. (**A**). Inflammatory infiltrates: diffuse inflammatory infiltrates were observed from 7 to 56 dpi. Scale bar: 50 µm. (**B**). Amastigote nests: amastigote nests were detected in the cardiac tissues of infected animals at 10, 14, and 21 dpi. Scale bar: 20 µm.

Table 2. Histopathological evaluation of cardiac tissue.

Group	Inflammation Score [1]	Amastigote Nests
Uninfected control	Absence	Absence
7 dpi	Mild	Absence
10 dpi	Moderate	Presence
14 dpi	Severe	Presence
21 dpi	Severe	Presence
56 dpi	Mild	Absence

[1] Inflammation score based on the type and number of inflammatory foci observed in both ventricles of BALB/c mice infected with 50,000 trypomastigotes per animal of the *T. cruzi* Dm28c strain. The score was determined by averaging six 20× fields per section across 3–4 sections per animal at different time points from 7 to 56 days post-infection (dpi) (n = 3/6, per group).

3.3. Splenomegaly Induced by Dm28c Infection Paired with Parasitemia Profile

Given the spleen's pivotal role in immune surveillance and parasite control, we evaluated its size throughout infection with the Dm28c strain. Splenomegaly was evident in infected animals as early as 7 dpi. Spleen weight progressively increased during infection, peaking at 14 dpi with a mean weight of 516.1 ± 8505 mg (mean ± SD), representing nearly a 7-fold increase compared to uninfected controls (Figure 3). Thereafter, spleen size gradually decreased, reaching values comparable to those observed at 7 dpi at 56 dpi.

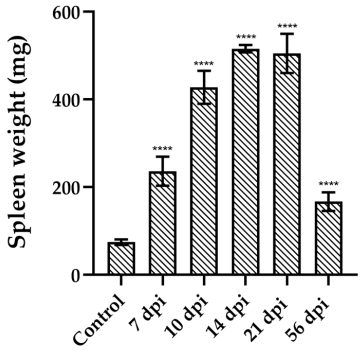

Figure 3. Spleen weight variations during *T. cruzi* Dm28c infection. Spleen weight was measured at different days post-infection (dpi). Data are presented as mean ± SD (n = 3–6 per group). Statistical analysis was performed using one-way ANOVA followed by Tukey's multiple comparisons test. **** $p < 0.0001$.

3.4. Splenic Pro- and Anti-Inflammatory Cytokine Gene Expression Patterns May Influence Infection Progression

To better characterize this inflammatory response, we evaluated the mRNA levels of pro- and anti-inflammatory cytokines in the spleen by RT-qPCR. Animals showed an increased expression of IFN-γ from 7 to 10 dpi and then a decrease during the rest of the infection, as shown in Figure 4. A similar pattern was observed for IL-1β, which reached its maximum expression at 7 dpi and gradually decreased over time, although these changes were not statistically significant. TNF-α expression remained low until 21 dpi, where its levels significantly increased (** $p < 0.01$, Figure 4). On the other hand, IL-10 expression increased at 7 dpi and gradually declined, but IL-10 mRNA levels remained significantly elevated compared to uninfected animals (Figure 4). No changes were found in TGF-β levels during the acute phase.

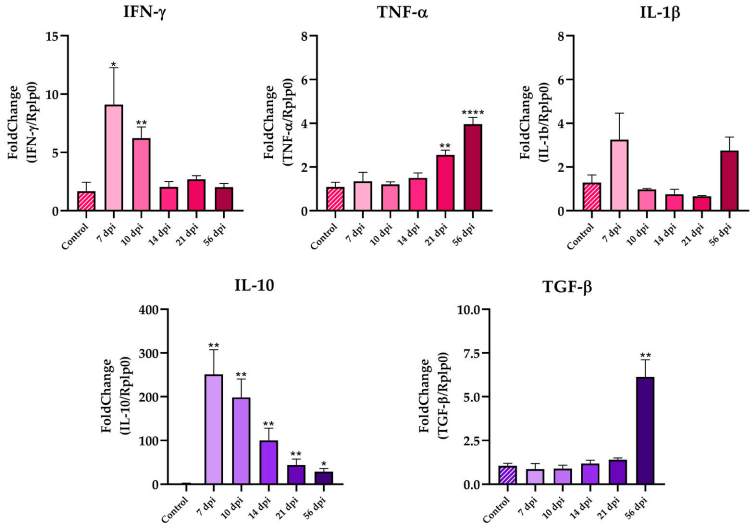

Figure 4. Expression analysis of IL-1β, TNF-α, IFN-γ, IL-10, and TGF-β in the spleen of mice infected with the Dm28c strain. Data was analyzed using the ΔΔCt method, normalized to the housekeeping

gene *rplp0* and expressed relative to the uninfected control. Results are presented as mean ± SEM. Statistical analysis was performed using an unpaired *t* test. * $p < 0.05$; ** $p < 0.01$, **** $p < 0.0001$.

4. Discussion

Animal models have been instrumental in unraveling the intricate host–parasite interactions that shape disease progression. Among the various factors influencing infection outcomes, the genetic diversity of *T. cruzi* and the host immune response are central. Experimental evidence from both clinical and laboratory studies supports the notion that disease manifestations result from the interplay between the parasite strain and the host genetic background. In this context, the immune system, particularly the balance between pro- and anti-inflammatory responses, plays a pivotal role. *T. cruzi* genetic diversity significantly influences pathogenicity, virulence, immune response, diagnosis, and treatment outcomes. From a clinical and epidemiological perspective, DTUs have been associated with varying symptomatology and disease progression. The infecting strain may influence the course of the disease, including the development of cardiac or digestive manifestations, or it may result in an asymptomatic state [6,18]. In this study, we established a murine experimental model using the *T. cruzi* Dm28c strain from DTU TcI to infect BALB/c mice, representing a low-virulence non-lethal Chagas disease model. The infection was characterized by an acute phase, where parasitemia can be detected by direct blood examination from 7 dpi, peaking at 14 dpi, and then decreasing to become undetectable by 56 dpi. Notably, despite the circulating trypomastigotes, animals maintained a healthy general state throughout the infection, showing no weight loss nor clinical manifestations such as piloerection, hunchback posture, or reduced mobility.

These findings clearly contrast with experimental models using other *T. cruzi* and/or mice strains. For example, the Tulahuen strain (TcVI) showed higher virulence and mortality in both C57BL/6 and BALB/c mice [19]. In both animal strains, parasitemia peaked at 21 dpi and loss of body weight, a marker of overall health status, was observed in accordance with a more severe acute phase. This lethal model showed 96% mortality between 21 and 25 dpi for C57BL/6 and 40% in the BALB/c strain. In contrast, in our model of Dm28c-infected BALB/c mice, 100% survival was observed. Also, previous studies showed that C57BL/6 mice were resistant to Dm28c infection, with undetectable parasitemia, which limited its usefulness for studying infection progression. Other low-virulence animal models of Chagas disease have been performed using the Sylvio X10/4 strain, which also belongs to DTU TcI [20]. Interestingly, although both Dm28c and Sylvio X10/4 belong to TcI, they behave differently in experimental models. Indeed, DTU TcI has its intrinsic variability, presents the broadest geographical distribution in the American continent, and has been associated with severe forms of cardiomyopathies. Cruz and co-workers observed significant differences between TcI domestic cycle-associated strains and sylvatic cycle-associated strains. While domestic strains presented higher parasitemias and low levels of histopathological damage, sylvatic strains showed lower parasitemias and significant levels of histopathological damage [21]. Despite their shared sylvatic origin, Dm28c and Sylvio X10/4 display divergent behaviors during infection. In contrast to Sylvio X10/4, whose bloodstream trypomastigotes are rarely detectable by microscopy and lead to chronic myocarditis in C3H/He mice [20], Dm28c parasites were observed in peripheral blood from BALB/c infected mice from 7 to 21 dpi and showed no signs of heart inflammation by 56 dpi. Additionally, it was observed that the severe chronic myocarditis seen in Sylvio-infected C3H/He mice was absent in C57BL/6, A/J, BALB/c, and DBA mice strains, suggesting that both parasites' genetic background and host genetics play critical roles in shaping the outcome of infection [20,22]. Regarding Dm28c, the infection of Swiss mice also exhibited a non-lethal infection, with a parasitemia peak at 23 dpi

and no significant changes in body weight or evidence of cardiac inflammatory infiltrates during a 77-day follow-up [23]. Histological analyses of cardiac tissues from BALB/c mice infected with Dm28c revealed diffuse lymphocytic infiltrates from 7 dpi and the presence of amastigote nests at the peak of parasitemia at 21 dpi. These manifestations were less severe than those observed in BALB/c- and C57BL/6-Tulahuen infections, which present well-defined inflammatory foci by 14 dpi and the presence of amastigote nests [19]. By 56 dpi, heart pathology in Dm28c-infected BALB/c mice appears to be resolved, and neither amastigote nests nor marked infiltrates were visible.

As previously mentioned, the distinct cardiac pathology observed among different mouse strains highlights the importance of host genetics in shaping disease outcome. Specifically, C3H/He and C57BL/6 mice exhibit differences in their immune responses that likely contribute to a divergent progression of *T. cruzi* infection. C3H/He mice are known to develop more robust Th1-type immune response, with higher production of IFN-γ and TNF-α, which may promote parasite control but also lead to increased immunopathology and severe acute myocarditis upon *T. cruzi* infection. In contrast, C57BL/6 mice exhibit a more balanced immune profile, with the presence of IFNγ^{+}IL-10^{+} $CD8^{+}$ T cells in cardiac tissue contributing to a controlled inflammatory response and milder pathology [24]. These immunological differences may explain the severe chronic myocarditis observed in C3H/He mice infected with Sylvio X10/4 compared to the milder cardiac phenotype in other strains.

Previous studies using strains such as Y, Colombiana, or CL Brener have demonstrated significant cardiac fibrosis [25,26]. In contrast, infections with low-virulence strains may show a slower or even self-limited progression toward fibrosis. In our model, no cardiac fibrosis was detected during the acute phase or at 56 dpi.

At the splenic level, BALB/c mice infected with Dm28c presented marked splenomegaly, with spleen weight peaking at 14 dpi, approximately 6.8 times larger than uninfected mice. Interestingly, this pattern mirrored parasitemia behavior, suggesting a direct relationship between parasite burden and splenic response. This expansion coincided with increased expression of pro-inflammatory cytokines, particularly IFN-γ and IL-1β, early during the acute phase, reflecting a predominant activation of the innate and Th1 immune axes. Simultaneously, elevated levels of the anti-inflammatory cytokine IL-10 were observed, likely as a compensatory regulatory mechanism aimed at mitigating tissue damage caused by excessive inflammation. A late increase in TNF-α and TGF-β was observed at 56 dpi, suggesting an ongoing modulation of the immune response. Indeed, although spleen weight was reduced at this point, it remained higher than uninfected mice. Given the spleen's central role in systemic immunity during acute *T. cruzi* infection, we analyzed cytokine expression at the mRNA level in this tissue to capture broader immune trends complementing heart histology. Although protein-level quantification (e.g., by ELISA) was not performed, the gene expression data provide a reliable overview of the dynamics of immune activation in this low-virulence infection model.

Our study demonstrates that the *T. cruzi* Dm28c strain induces a mild, non-lethal infection in BALB/c mice, which could be a good model to study evolution from the acute phase to an indeterminate or non-symptomatic chronic infection, enabling the analysis of disease progression. In contrast to more virulent strains like Tulahuen, Dm28c triggered a balanced immune response and caused limited tissue damage, with the partial resolution of pathology following the peak of parasitemia. This approach remains suitable for long-term follow-up and evaluation of chronic stages, and it remains a promising strategy to further explore immunological and pathological features of the chronic phase in future studies.

Our findings highlight the relevance of strain-dependent variability in experimental models of Chagas disease. We believe that our Dm28c-infected BALB/c model offers a valu-

able platform for investigating host–parasite interactions across disease stages. Moreover, it provides a suitable framework for evaluating diagnostic, therapeutic, and preventive strategies under low-virulence conditions and for simulating diverse epidemiological scenarios observed in endemic regions.

Author Contributions: Conceptualization, P.C. and S.R.V.; methodology, M.A.d.H. and S.R.V.; investigation, M.A.d.H., S.R.V. and P.C.; resources, S.R.V. and P.C.; writing—original draft preparation, M.A.d.H., S.R.V. and P.C.; writing—review and editing, M.A.d.H., S.R.V. and P.C.; funding acquisition, P.C. All authors have read and agreed to the published version of the manuscript.

Funding: This research was funded by the Agencia Nacional de Promoción de la Investigación, el Desarrollo Tecnológico y la Innovación (Agencia I+D+i), Argentina, grant numbers PICT 2016-0439 and PICT 2019-4212, and by the Consejo Nacional de Investigaciones Científicas y Técnicas (CONICET), Argentina, grant number PIP 2021-0848.

Institutional Review Board Statement: The animal study protocol was approved by the Institutional Animal Care & Use Committee of FACULTAD DE CIENCIAS MEDICAS, UNIVERSIDAD NACIONAL DE ROSARIO (Res. No. 2477/2016 date of approval 18 October 2016).

Data Availability Statement: The raw data supporting the findings of this study are openly available in the Universidad Nacional de Rosario Dataverse Repository (RDA-UNR) at the following DOI: https://doi.org/10.57715/UNR/TLENTW. URL (accessed on 10 July 2025).

Acknowledgments: We thank Technician. María Dolores Campos and Doctor Romina Manarín for their valuable assistance with cell and parasite culture techniques, as well as Licenciado Facundo Rojas for his technical support at the IBR. We are also grateful to the members of the Histotechnology Service at FBIOyF, UNR, Histotechnicians Alejandra Quintana and Diego Parenti, for their essential contributions.

Conflicts of Interest: The authors declare no conflicts of interest. The funders had no role in the design of the study; in the collection, analyses, or interpretation of data; in the writing of the manuscript; or in the decision to publish the results.

Abbreviations

The following abbreviations are used in this manuscript:

dpi	Days post-infection
DTU	Discrete Typing Unit
FCS	Fetal calf serum
IFN-γ	Interferon gamma
IL-10	Interleukin-10/human cytokine synthesis inhibitory factor
IL-1β	Interleukin-1 beta
mRNA	Message RNA
PBS	Phosphate-buffered saline
TGF-β	Transforming growth factor β
TNF-α	Tumoral necrosis factor alfa

Appendix A. Histological Assessment of Cardiac Fibrosis

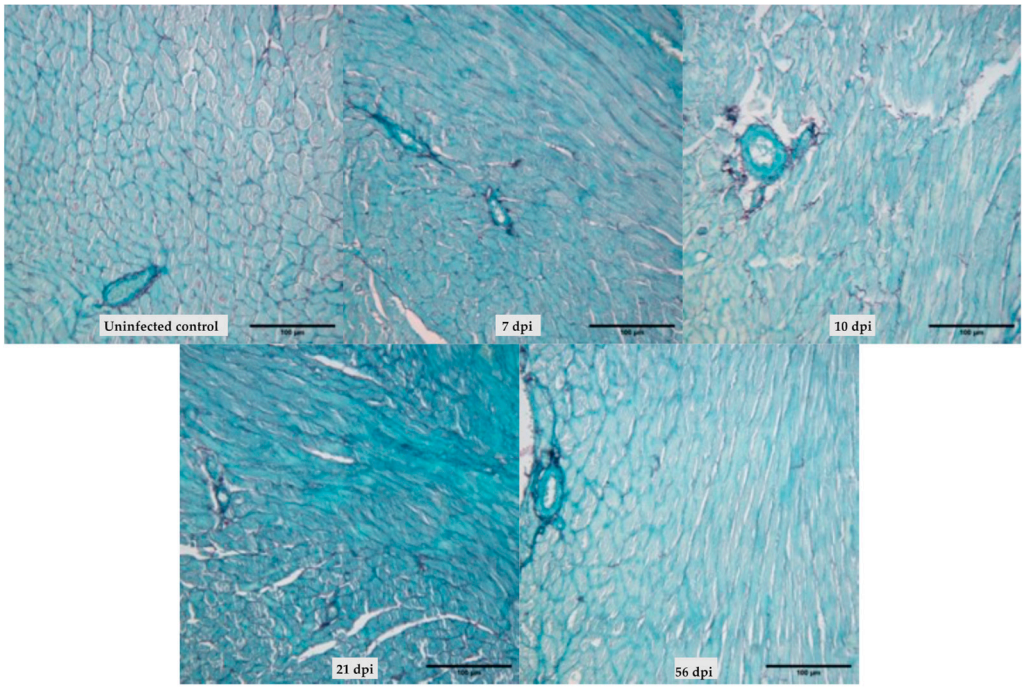

Figure A1. Histological analysis of cardiac fibrosis in *T. cruzi* Dm28c-infected mice. Representative cardiac sections from BALB/c mice infected with 50,000 trypomastigotes of the *T. cruzi* Dm28c strain, stained with Picrosirius Red/Fast Green to evaluate collagen deposition. No fibrotic remodeling was observed at any of the analyzed time points (7, 10, 21, and 56 dpi). Red staining indicates collagen fibers; green staining corresponds to non-collagenous tissue. Scale bar: 100 µm.

References

1. Word Health Organization (WHO). Chagas Disease (Also Known as American Tripanomiasis). Available online: https://www.who.int/news-room/fact-sheets/detail/chagas-disease-(american-trypanosomiasis) (accessed on 10 July 2025).
2. Coura, J.R.; Viñas, P.A. Chagas Disease: A New Worldwide Challenge. *Nature* **2010**, *465*, S6–S7. [CrossRef]
3. Nunes, M.C.P.; Dones, W.; Morillo, C.A.; Encina, J.J.; Ribeiro, A.L. Chagas Disease. *J. Am. Coll. Cardiol.* **2013**, *62*, 767–776. [CrossRef]
4. Bermudez, J.; Davies, C.; Simonazzi, A.; Pablo Real, J.; Palma, S. Current Drug Therapy and Pharmaceutical Challenges for Chagas Disease. *Acta Trop.* **2016**, *156*, 1–16. [CrossRef] [PubMed]
5. Martinez, S.J.; Romano, P.S.; Engman, D.M. Precision Health for Chagas Disease: Integrating Parasite and Host Factors to Predict Outcome of Infection and Response to Therapy. *Front. Cell. Infect. Microbiol.* **2020**, *10*, 210. [CrossRef] [PubMed]
6. Zingales, B. *Trypanosoma cruzi* Genetic Diversity: Something New for Something Known about Chagas Disease Manifestations, Serodiagnosis and Drug Sensitivity. *Acta Trop.* **2018**, *184*, 38–52. [CrossRef] [PubMed]
7. Zingales, B.; Bartholomeu, D.C. *Trypanosoma cruzi* Genetic Diversity: Impact on Transmission Cycles and Chagas Disease. *Mem. Do Inst. Oswaldo Cruz* **2022**, *117*, e210193. [CrossRef]
8. Zingales, B.; Macedo, A.M. Fifteen Years after the Definition of *Trypanosoma cruzi* DTUs: What Have We Learned? *Life* **2023**, *13*, 2339. [CrossRef]
9. Velásquez-Ortiz, N.; Herrera, G.; Hernández, C.; Muñoz, M.; Ramírez, J.D. Discrete Typing Units of *Trypanosoma cruzi*: Geographical and Biological Distribution in the Americas. *Sci. Data* **2022**, *9*, 360. [CrossRef]
10. Revollo, S.; Oury, B.; Vela, A.; Tibayrenc, M.; Sereno, D. In Vitro Benznidazole and Nifurtimox Susceptibility Profile of *Trypanosoma cruzi* Strains Belonging to Discrete Typing Units TcI, TcII, and TcV. *Pathogens* **2019**, *8*, 197. [CrossRef]
11. Talvani, A.; Teixeira, M.M. Experimental *Trypanosoma cruzi* Infection and Chagas Disease—A Word of Caution. *Microorganisms* **2023**, *11*, 1613. [CrossRef]
12. Goldenberg, S.; Contreras, V.T.; Salles, J.M.; Bonaldo, M.C.; de Lima Franco, M.P.A.; Linss, J.; Lafaille, J.; Valle, D.; Morel, C.M. Facts and Hypothesis on *Trypanosoma cruzi* Differentiation. *Memórias Do Inst. Oswaldo Cruz* **1984**, *79*, 39–44. [CrossRef]

13. Ferreira, B.L.; Ferreira, É.R.; De Brito, M.V.; Salu, B.R.; Oliva, M.L.V.; Mortara, R.A.; Orikaza, C.M. BALB/c and C57BL/6 Mice Cytokine Responses to *Trypanosoma cruzi* Infection Are Independent of Parasite Strain Infectivity. *Front. Microbiol.* **2018**, *9*, 553. [CrossRef] [PubMed]
14. Tavernelli, L.E.; Motta, M.C.M.; Gonçalves, C.S.; Da Silva, M.S.; Elias, M.C.; Alonso, V.L.; Serra, E.; Cribb, P. Overexpression of *Trypanosoma cruzi* High Mobility Group B Protein (TcHMGB) Alters the Nuclear Structure, Impairs Cytokinesis and Reduces the Parasite Infectivity. *Sci. Rep.* **2019**, *9*, 192. [CrossRef]
15. Brener, Z. Therapeutic Activity and Criterion of Cure on Mice Experimentally Infected with *Trypanosoma cruzi*. *Rev. Do Inst. Med. Trop. São Paulo* **1962**, *4*, 389–396.
16. Pérez, A.R.; Lambertucci, F.; González, F.B.; Roggero, E.A.; Bottasso, O.A.; de Meis, J.; Ronco, M.T.; Villar, S.R. Death of Adrenocortical Cells during Murine Acute *T. Cruzi* Infection Is Not Associated with TNF-R1 Signaling but Mostly with the Type II Pathway of Fas-Mediated Apoptosis. *Brain Behav. Immun.* **2017**, *65*, 284–295. [CrossRef]
17. Mishra, P.; Singh, U.; Pandey, C.M.; Mishra, P.; Pandey, G. Application of Student's *t*-Test, Analysis of Variance, and Covariance. *Ann. Card. Anaesth.* **2019**, *22*, 407–411. [CrossRef]
18. Silvestrini, M.M.A.; Alessio, G.D.; Frias, B.E.D.; Sales Júnior, P.A.; Araújo, M.S.S.; Silvestrini, C.M.A.; Brito Alvim De Melo, G.E.; Martins-Filho, O.A.; Teixeira-Carvalho, A.; Martins, H.R. New Insights into *Trypanosoma cruzi* Genetic Diversity, and Its Influence on Parasite Biology and Clinical Outcomes. *Front. Immunol.* **2024**, *15*, 1342431. [CrossRef]
19. Roggero, E.; Perez, A.; Tamae-Kakazu, M.; Piazzon, I.; Nepomnaschy, I.; Wietzerbin, J.; Serra, E.; Revelli, S.; Bottasso, O. Differential Susceptibility to Acute *Trypanosoma cruzi* Infection in BALB/c and C57BL/6 Mice Is Not Associated with a Distinct Parasite Load but Cytokine Abnormalities. *Clin. Exp. Immunol.* **2002**, *128*, 421–428. [CrossRef]
20. Marinho, C.R.F.; Nuñez-Apaza, L.N.; Bortoluci, K.R.; Bombeiro, A.L.; Bucci, D.Z.; Grisotto, M.G.; Sardinha, L.R.; Jorquera, C.E.; Lira, S.; D'Império Lima, M.R.; et al. Infection by the Sylvio X10/4 Clone of *Trypanosoma cruzi*: Relevance of a Low-Virulence Model of Chagas' Disease. *Microbes Infect.* **2009**, *11*, 1037–1045. [CrossRef]
21. Cruz, L.; Vivas, A.; Montilla, M.; Hernández, C.; Flórez, C.; Parra, E.; Ramírez, J.D. Comparative Study of the Biological Properties of *Trypanosoma cruzi* I Genotypes in a Murine Experimental Model. *Infect. Genet. Evol.* **2015**, *29*, 110–117. [CrossRef] [PubMed]
22. Marinho, C.R.F.; Bucci, D.Z.; Dagli, M.L.Z.; Bastos, K.R.B.; Grisotto, M.G.; Sardinha, L.R.; Baptista, C.R.G.M.; Penha Gonçalves, C.; Lima, M.R.D.; Álvarez, J.M. Pathology Affects Different Organs in Two Mouse Strains Chronically Infected by a *Trypanosoma cruzi* Clone: A Model for Genetic Studies of Chagas' Disease. *Infect. Immun.* **2004**, *72*, 2350–2357. [CrossRef]
23. Calvet, C.M.; Meuser, M.; Almeida, D.; Meirelles, M.N.L.; Pereira, M.C.S. *Trypanosoma cruzi*–Cardiomyocyte Interaction: Role of Fibronectin in the Recognition Process and Extracellular Matrix Expression in Vitro and in Vivo. *Exp. Parasitol.* **2004**, *107*, 20–30. [CrossRef]
24. Roffê, E.; Rothfuchs, A.G.; Santiago, H.C.; Marino, A.P.M.P.; Ribeiro-Gomes, F.L.; Eckhaus, M.; Antonelli, L.R.V.; Murphy, P.M. IL-10 Limits Parasite Burden and Protects against Fatal Myocarditis in a Mouse Model of *Trypanosoma cruzi* Infection. *J. Immunol.* **2012**, *188*, 649–660. [CrossRef] [PubMed]
25. Coelho, L.L.; Pereira, I.R.; de Souza Pereira, M.C.; Mesquita, L.; Lannes-Vieira, J.; Adesse, D.; Garzoni, L.R. *Trypanosoma cruzi* Activates Mouse Cardiac Fibroblasts in Vitro Leading to Fibroblast-Myofibroblast Transition and Increase in Expression of Extracellular Matrix Proteins. *Parasit Vectors* **2018**, *11*, 72. [CrossRef] [PubMed]
26. De Alba-Alvarado, M.; Bucio-Torres, M.I.; Zenteno, E.; Sampedro-Carrillo, E.; Hernández-Lopez, M.; Reynoso-Ducoing, O.; Torres-Gutiérrez, E.; Guevara-Gomez, Y.; Guerrero-Alquicira, R.; Cabrera-Bravo, M.; et al. Response to Infection by *Trypanosoma cruzi* in a Murine Model. *Front. Vet. Sci.* **2020**, *7*, 568745. [CrossRef] [PubMed]